



## The Relationship between the Anticyclonic Anomalies in Northeast Asia and Severe Haze in the Beijing-Tianjin-Hebei Region

Wogu Zhong <sup>1,2</sup>, Zhicong Yin <sup>1,2\*</sup> and Huijun Wang <sup>1,2</sup>

<sup>1</sup>Key Laboratory of Meteorological Disaster, Ministry of Education / Joint International Research Laboratory of Climate and Environment Change (ILCEC) / Collaborative Innovation Center on Forecast and Evaluation of Meteorological Disasters (CIC-FEMD), Nanjing University of Information Science & Technology, Nanjing 210044, China

<sup>2</sup>Nansen-Zhu International Research Centre, Institute of Atmospheric Physics, Chinese Academy of Sciences, Beijing, China

\*Correspondence to: Zhicong Yin (yinzhc@163.com)

**Abstract.** Haze pollution in the Beijing-Tianjin-Hebei (BTH) region has become increasingly more severe and persistent in recent years. To better understand the formation of severe haze and its relationship with anticyclonic anomalies over Northeast Asia (AANA), this research focused on severe haze over the BTH region occurring in December during 2014-2016 and examined the impacts of the AANA. The results indicated that local meteorological conditions were conducive to severe haze (such as weaker surface wind, stronger temperature inversion, lower boundary layer and higher relative humidity) and were all closely related to the AANA. During severe haze episodes, the AANA remained strong in the mid-upper troposphere, which caused anomalous southerly wind. From the horizontal direction, strong southeasterly wind promoted the accumulation of pollutants and moisture while generating temperature inversion layer. The AANA also induced anomalous ascending motion over the BTH region, which broke the local meridional circulation. This restricted clean air from sinking to the surface and directly led to severe haze. The downward transportation of westerly momentum was also restrained, resulting in weaker surface wind and shallower boundary layer. The indirect zonal circulation between the BTH region and western Pacific triggered by the AANA provided a stable source of moisture to the BTH region, which strengthened the development of severe haze by promoting the growth of fine particles and weakening turbulence. The advance and retreat of the AANA were corresponded with the emergence and dissipation of severe haze, illustrating that the AANA could be an effective forecast indicator for air quality.

**Key words:** severe haze pollution; PM<sub>2.5</sub>; anticyclonic anomalies; air quality

### 1. Introduction

In recent years, the Beijing-Tianjin-Hebei (BTH, located at 36°-42°N, 114°-120°E) region has witnessed several severe haze events with the characteristics of long duration, wide range and serious pollution level, which are detrimental to people's life and health (Hu et al., 2015; Wang et al., 2016). Notably, the number of haze days in the BTH region have increased, and



the affected area has shown an interdecadal expanding trend (Zhang et al., 2015). To control the air pollution, the Chinese government promulgated the Air Pollution Prevention and Control Action Plan in 2013. So far, the atmospheric environment quality in the BTH region has improved to a certain extent, mainly for the reduction in SO<sub>2</sub> and NO<sub>2</sub> concentrations (“Formation Mechanism and Control Strategies of Haze in China” professional group, 2015). However, the decline in PM<sub>2.5</sub> concentration was not obvious, and haze events still occurred with increasing frequency, especially in the winter. During 16-21 December 2016, the BTH region suffered serious air pollution. Despite more than 30 cities initiating an air pollution red alert ahead of time, the pollution lasted for five days, and the instantaneous PM<sub>2.5</sub> concentration reached up to 1000 µg · m<sup>-3</sup> in Shijiazhuang, the capital of Hebei province. Another pollution event occurred from 30 December 2016 to 7 January 2017, lasting for as long as nine days. These two long-term severe haze processes were detected within 20 days, which triggered a broader discussion over their formation, scientific attribution and reasonable methods of management (Wang, 2018).

Previous studies have indicated that the formation of severe haze is characterized by a complex interplay between anthropogenic emissions, chemical processes and meteorological factors (Wang et al., 2016; Liu et al., 2017; Tang et al., 2018). The basic reason of haze pollution is excessive emission (Wang et al., 2013; Zhang et al., 2013). The synergistic effect of these anthropogenic emissions may worsen air pollution in North China (Wang et al., 2016; Yang et al., 2016). Nevertheless, meteorological conditions still play a key role in the formation of haze events (Zhang et al., 2014; Yin and Wang, 2017a; Wei et al., 2017). According to recent research (Cai et al., 2017), atmospheric circulation changes induced by global warming may enhance the stability of the lower atmosphere in Beijing, leading to more frequent and severe haze pollution in the future. Furthermore, the decline of autumn Arctic sea ice and the negative anomalies of subtropical western Pacific sea surface temperature could greatly change the atmospheric circulation and lead to an increase in haze days in eastern China (Wang et al., 2015; Yin and Wang, 2016). Haze pollution could be exacerbated under these preceding force factors through their impacts on atmospheric circulations and meteorological conditions. In addition, local meteorological conditions and the structure of boundary layer will vary with the change in the large-scale circulation conditions, which could affect the dispersion capability of atmosphere and thus have an effect on air pollution (Wu et al., 2017). The weather conditions affecting pollutant dispersion include dynamic factors (e.g., wind and turbulence) and thermodynamic factors (e.g., atmospheric stratification and its stability) (Zhang et al., 2014). Lower wind speed, higher relative humidity and stable atmospheric stratification are the main factors that are conducive to the occurrence of haze (Zhang et al., 2014; Ding and Liu, 2014; Yin et al., 2015b). Such weather conditions could be strengthened by the weaker East Asian winter monsoon and the positive phase of the East Atlantic-West Russia (EA/WR) teleconnection (Yin et al., 2015a; Wu et al., 2016; Yin and Wang, 2016).

Research on persistent and severe haze pollution in the BTH region has demonstrated that the anticyclonic anomalies in Northeast Asia (AANA) represent a key local circulation that is conducive to the formation of serious haze pollution. Some studies indicated that weak East Asian winter monsoon (EAWM) could modulate the AANA (Li et al. 2015; Yin et al. 2015a).



With the decline of EAWM, cold air is restricted to high-latitude areas, and the East Asian trough becomes weak. It is physically reasonable that the weaker East Asian trough appears as anticyclonic circulations in the anomaly field. Thus, to some extent, the AANA is a representative indicator of EAWM systems (Wang and Jiang, 2004). However, it is still unclear how such atmospheric anomalies affect the severe haze events. To better represent the intensity of the AANA and its physical mechanism on haze pollution, we defined  $AANA_{I_{Z500}}$  ( $AANA_{I_{\omega 500}}$ ) and  $AANA_{I_{V850}}$  according to the composite anomalies at 500 hPa geopotential (vertical velocity) field and 850 hPa wind field on severe haze episodes, referring to previous EAWM indexes (Wang and Jiang, 2004; He and Wang, 2012). This study focused on the severe haze in the BTH region during the period of December 2014-2016 and explicated the characteristics of the AANA and its relationship with severe haze, while making comparison with non-haze episodes.

## 2. Data and method

Meteorological observation data at three-hour intervals in December 2014-2016 were obtained from China Meteorological Administration, including visibility, surface wind speed and surface relative humidity. Hourly  $PM_{2.5}$  concentration data of 80 national air quality stations over the BTH region were derived from the website of Ministry of Ecology and Environment of China. Additionally, the geopotential height at 500 hPa, sea level pressure (SLP), U and V components of wind at 200 hPa, 850 hPa and the surface, vertical wind (omega) from 200 hPa to 1000 hPa, temperature at 925 hPa, 1000 hPa and the surface, surface dew point temperature, relative humidity from 200 hPa to 1000 hPa, and planetary boundary layer height (PBLH) from the ERA-Interim reanalysis data were downloaded from the European Centre for Medium-Range Weather Forecasts (ECMWF), with a horizontal resolution of  $0.75^\circ \times 0.75^\circ$ . The distribution data of surface relative humidity were calculated by the surface temperature and dew point temperature from the ERA-Interim reanalysis data.

Considering that national air quality stations over the BTH region are scarce and unevenly distributed, here we created Thiessen polygon to calculate the weighted average of  $PM_{2.5}$  concentration and built the time series at intervals of six hours. Then, we selected the severe haze events (defined as  $PM_{2.5}$  concentration  $\geq 150 \mu\text{g} \cdot \text{m}^{-3}$ ; Cai et al., 2017) and non-haze events ( $PM_{2.5}$  concentration  $\leq 50 \mu\text{g} \cdot \text{m}^{-3}$ ) and used composite analysis to analyze the associated atmospheric circulations and weather conditions. Most previous studies investigated haze events in units of hours or days and the variations among haze progresses were not taken into account. Some meteorological factors might be closely related to haze pollution in a few cases but remained insignificant in others. In this way, the relationship between haze pollution and meteorological factors might be overemphasized. To better describe the relationships and mechanisms manifesting among different synoptic processes, new data called synoptic process mean (SPM) data were rebuilt. According to the  $PM_{2.5}$  concentration, the synoptic processes were divided into three groups: severe haze, non-haze and non-severe haze (i.e.,  $PM_{2.5}$  concentration  $\in [50, 150] \mu\text{g} \cdot \text{m}^{-3}$ ). The SPM data applied time averaging method to calculate the mean  $PM_{2.5}$  concentration and meteorological data during each



process. Based on the SPM data, the synoptic process correlation coefficients (SPCCs) were calculated in the units of synoptic processes, rather than in units of hours or days. This method maintains the physical relations between haze and meteorological factors while removing the strong correlation inside each process. In addition, the vertical transport of westerly momentum was defined as  $\frac{\partial u\omega}{\partial p}$  in this study (Zhong et al., 2010).  $\frac{\partial u\omega}{\partial p} < 0$  represents the downward transport of westerly momentum, and  $\frac{\partial u\omega}{\partial p} > 0$  represents the upward transport of westerly momentum (i.e., the downward transport was restricted).

### 3. Results

Figure 1 shows the six-hour variation of  $\text{PM}_{2.5}$  concentration over the BTH region in December 2014-2016. The monthly mean concentrations in 2014-2016 were  $84.7 \mu\text{g} \cdot \text{m}^{-3}$ ,  $126.4 \mu\text{g} \cdot \text{m}^{-3}$ , and  $128.1 \mu\text{g} \cdot \text{m}^{-3}$ , and the standard deviations were  $55.4 \mu\text{g} \cdot \text{m}^{-3}$ ,  $79.1 \mu\text{g} \cdot \text{m}^{-3}$ , and  $70.9 \mu\text{g} \cdot \text{m}^{-3}$ , respectively. These results demonstrated that haze pollutions in December were serious and fluctuated strongly. The first and third quartiles of the series were  $54.0 \mu\text{g} \cdot \text{m}^{-3}$  and  $156.7 \mu\text{g} \cdot \text{m}^{-3}$ , indicating that the threshold values of severe haze ( $150 \mu\text{g} \cdot \text{m}^{-3}$ ) and non-haze ( $50 \mu\text{g} \cdot \text{m}^{-3}$ ) events were reasonable. There were 18 severe haze and 20 non-haze events in December 2014-2016 (Table 1). The duration time of severe haze events was relatively longer than that of non-haze events, especially in 2015 and 2016. Severe haze broke out rapidly in most cases, but the dissipation processes varied in different years. The  $\text{PM}_{2.5}$  concentration decreased quickly in 2014, while it remained at high concentration levels before lowering down in 2015 and 2016. Thus, severe haze had the tendency of becoming more persistent during the period of 2014-2016. Specific to the severe haze since 15 December 2016, most cities in the BTH region and the surrounding areas issued an air pollution red alert ahead of time, and anthropogenic discharges were strictly controlled. Despite those efforts, the BTH region was still hit by serious and persistent haze, demonstrating that meteorological conditions had a significant impact on haze pollution (Yin and Wang, 2017b).

As a critical system influencing the climate pattern over East Asia, EAWM plays an important role in the formation of severe haze (Zhang et al., 2014; Yin et al., 2015; Yin and Wang, 2017b). When severe haze occurred, the EAWM weakened from the upper to the lower troposphere, which could be verified by the negative patterns over the Siberia and the Aleutian Islands at the mid-level (Figure 2a), the decline in northerly wind near the surface (Figure 3a–b) and warmer land surface (Figure 2b). As a consequence, the East Asian jet stream was weaker and moved northward with respect to the climatological mean (Yin and Wang, 2017b), while the East Asian trough declined and moved eastwards (Figure 2a). These results indicated that the meridional circulation over the middle-high latitude area in East Asia was weakened and that the BTH region was mainly occupied by zonal circulation. Thus, the cold air stayed inactive, and its frequency of moving southward and entering into the BTH region decreased (Chen and Wang, 2015; Yin and Wang, 2017b). The decline in prevailing northerly wind near the surface was strengthened by the reduction in the land-sea pressure differences. The negative anomalies of the SLP were obvious over the middle-high latitude area in the Eurasian continent, with two meions located in the Siberian plain and Bering



125 Strait, while the SLP in the Western Pacific was a positive anomaly (Figure 2b). The change in differences between land and sea induced southeasterly wind, restricting the dispersion of pollutants. Moreover, the warm air brought by southeaster strengthened the intensity of temperature inversion potential (TIP,  $T_{925}-T_{1000}$ ). The emergence of stable stratification restricted the vertical dispersion of pollutants (Figure 3a). When it came to non-haze events, the EAWM was relatively strong in the troposphere (Figure 2c–d). Thus, the cold air activity became more frequent, resulting in stronger surface wind and lower surface relative humidity in the BTH region (Figure 3c–d). In addition, the pressure differences between the Western Pacific and BTH region increased relatively, and the northerly wind was strengthened, accelerating the decrease in the  $PM_{2.5}$  concentration. In general, the weakening of the EAWM restricted the cold air activity and had an impact on local weather conditions, including surface wind speed, surface relative humidity and TIP, whose SPCCs with the mean  $PM_{2.5}$  concentration in the BTH region were -0.41, 0.73 and 0.63, respectively, and all exceeded the 99% confidence level (Table 2). With the decline in the wind speed near the surface and the increase in the TIP, the horizontal and vertical dispersion abilities of the pollutants decreased, while higher surface relative humidity exacerbated the formation of contaminants. These factors led to a rapid increase in the  $PM_{2.5}$  concentration and resulted in severe haze (Figure 4).

135 The mentioned southeasterly wind, abundant moisture and strong temperature inversion that induced severe haze were all closely related to the AANA (Figure 4–5). Thus, we evaluated the AANA as the marked influencing atmospheric circulation. Here, we defined three indexes:  $AANAI_{Z500}$  (defined as  $Z_{500}$  anomalies over 115–140°E, 30–50°N, i.e., the white box in Figure 2a),  $AANAI_{V850}$  (defined as wind speed anomalies at 850 hPa over 120–150°E, 30–40°N, i.e., the black box in Figure 3a) and  $AANAI_{\omega 500}$  (defined as  $\omega_{500}$  anomalies over 115–125°E, 35–45°N, i.e., the white box in Figure 6a) to describe the intensity of the AANA in the mid and lower troposphere. Note that the  $AANAI_{Z500}$  and  $AANAI_{V850}$  were similar to previous EAWM indexes (Wang and Jiang, 2004; He and Wang, 2012) since the AANA was an important manifestation of the weaker EAWM (Figure 2a). However, here we defined these indexes through the anomaly field to analyze anomalous atmospheric circulation, differing from the EAWM indexes, which were used to describe the intensity of the EAWM and its climatic evolution. The physical meaning and the critical areas taking into account were different between the  $AANAI_{Z500}$  ( $AANAI_{V850}$ ) and EAWM indexes. 145 Considering that the  $AANAI_{Z500}$  and  $AANAI_{V850}$  only represented the intensity of the AANA from the horizontal direction, we further introduced  $AANAI_{\omega 500}$  to investigate the vertical structure of the AANA. This part will be illustrated in detail in the following section. We calculated the SPCC between the mean  $PM_{2.5}$  concentration in the BTH region and the  $AANAI_{Z500}$  ( $AANAI_{V850}$ ), and it was 0.57 (-0.64), exceeding the 99% confidence level (Table 2). Thus, the AANA could affect the emergence and development of severe haze (Figure 5). When severe haze took place, the AANA could be identified from the lower to the upper troposphere, especially at the mid-level (Figure 6a). From the horizontal direction, the AANA could generate southeasterly wind near the surface (Figure 3a). Considering that the BTH region is located in the southeast of Taihang-Yanshan mountain, the anomalous southeaster was beneficial to the accumulation of pollutants and water vapor. Southeasterly wind 150



gathered pollutants from the surrounding area and provided a steady supply of haze particles while bringing moisture from the Western Pacific to the Bohai Bay. With the weak convergence aroused by the anomalous low surface pressure, moisture was transported to the BTH region (Figure 3b). This promoted the hygroscopic growth of fine particles and the formation of secondary pollutants (Wang et al, 2016). In addition, the warm advection over the BTH region induced by the southeasterly wind could be verified in the middle and lower troposphere (Figure 7). Strong warm advection at the mid-level was consistent with the decline in the EAWM. Specifically, the warm advection at 950 hPa was relatively stronger than that at 1000 hPa. This was propitious to the formation of temperature inversion layer and the increase in atmospheric stability (Figure 3a). The SPCC between the  $AANA_{I_{Z500}}$  and TIP was 0.39 and exceeded the 99% confidence level (Table 3). For non-haze events, Northeast Asia was mainly controlled by cyclonic anomalies (Figure 6b), which strengthened the northerly wind near the surface (Figure 3c). Strong northerly wind brought about cold advection over the BTH region and restrained the transport of water vapor (Figure 3d). Higher wind speed and drier atmosphere were conducive to the dispersion of pollutants. The SPCC between the  $AANA_{I_{Z500}}$  and surface wind speed (surface relative humidity) was -0.41 (0.65), exceeding the 99% confidence level (Table 3). Thus, because of the special topography condition in the BTH region, the anomalous southeasterly wind caused by the AANA facilitated the formation and aggregation of haze particles. The emergence of temperature inversion layer enhanced the atmospheric stability, leading to more persistent and serious haze events. Aside from horizontal dispersion, vertical dispersion also played a vital role in haze pollution (Zhao et al, 2013; Wu et al, 2017). When severe haze occurred, the negative anomalies of vertical velocity ( $\omega$ ) were verified in Northeast Asia and coastal regions of eastern China, while positive anomalies were mainly located in Northwestern Pacific (Figure 6a). Thus, the AANA at the mid-level stimulated the anomalous ascending motion in the rear and descending motion in the front. The distribution of anomalies was opposite in non-haze events: cyclonic anomalies appeared with ascending motion in the front and descending motion in the rear (Figure 6b). In particular, the SPCC between the  $AANA_{\omega_{500}}$  and the mean  $PM_{2.5}$  concentration in the BTH region was -0.60, exceeding the 99% confidence level (Table 2). This result demonstrated that the ascending motion at the back of the AANA had a significant effect on haze pollution in the BTH region. Our results appeared to have a conflict with the insufficient speculation by Yin and Wang (2017b). The following sections would explain how the associated vertical circulation affected severe haze in the BTH region.

The anomalous ascending motion generated by the AANA had a broad range in the troposphere (Figure 8). This vertical flow led to wind anomalies in the synoptic processes, which appeared as weak and narrow ascending motion in the lower troposphere (Figure 9a). Thus, the normal meridional circulation in the local area (Figure S1) was broken. The descending motion from the upper level was restrained at 500-800 hPa. The confrontation between updraft and downdraft restricted the transportation of dry and clean air from the upper atmosphere to the surface, which directly led to the formation of severe haze (Sun et al., 2017). Actually, the strong warm advection mentioned above represented the decline in the dry air intrusion (Sun et al., 2017), which could be verified in Figure 7. Furthermore, the anomalous ascending motion in the middle-upper



185 atmosphere confined the downward transportation of westerly momentum (i.e.,  $\frac{\partial u\omega}{\partial p} > 0$ , Figure 9b), which led to weaker  
surface wind speed (Lu et al., 2010). The inhibited downward momentum could also affect the intensity of turbulence. On one  
hand, with the weakening of momentum exchange between the upper and lower atmosphere, the transformation of kinetic  
energy from the basic flow to the turbulent flow was restrained (Liu et al., 2011). On the other hand, the temperature inversion  
generated by AANA would lead to the increase in atmospheric stability and dissipate the turbulent kinetic energy. In this  
190 situation, the kinetic energy of turbulence decreased (Liu et al., 2011), which would lead to weaker turbulence and have adverse  
effects on the dispersion of pollutants. This could be verified by the overall weak meridional circulation in the synoptic  
processes (Figure 9a). Meanwhile, the weak turbulence resulted in a shallower planetary boundary layer (PBL) and reduced  
the atmospheric environment capacity. The SPCC between the AANA<sub>I2500</sub> and PBLH anomalies was -0.48, passing the 99%  
confidence level (Table 3). The height of the PBL was approximately 200 m lower than the climatological mean from 36° to  
42°N (i.e., the BTH region, Figure 8a), whose SPCC with the PM<sub>2.5</sub> concentration was -0.38 and exceeded the 99% confidence  
195 level (Table 2). Therefore, the decline in the PBLH triggered serious and persistent haze. For the non-haze episodes, the strong  
sinking motion was obvious in the troposphere (Figure 8c–d), which represented the downward transport of westerly  
momentum and the clean air (Figure 9c–d). Under these circumstances, surface wind speed and turbulent exchange  
strengthened, leading to conducive conditions for pollutant dispersion. In general, the AANA generated ascending motion in  
its rear, which broke the normal meridional circulation in the BTH region and restricted the clean air in the upper troposphere  
200 from sinking to the surface. This effect was the proximate cause of severe haze in the BTH region. The ascending motion also  
restrained the transportation of downward momentum and led to the conditions of lower surface wind speed, weaker turbulence  
and shallower PBL in the local area, which were conducive to the formation and development of severe haze.

Note that the AANA motivated an indirect zonal circulation between the BTH region and Western Pacific, which acted  
as an important water vapor path (Figure 8b). The easterly wind in the lower troposphere triggered by the AANA brought  
205 humid and warm air to the BTH region and resulted in higher relative humidity in the lower (900 hPa) atmosphere. This could  
accelerate the growth of fine particles and lead to a sharp increase in PM<sub>2.5</sub> concentration. Higher relative humidity near the  
surface also restrained evaporation. Consequently, ascending motion in the lower level declined, which restricted the  
development of turbulence (Betts, 1997). Moreover, warm air from the ocean generated advection inversion when it moved to  
the land. The development of thermal inversion led to weaker turbulence, which limited the ascending motion in the lower  
210 levels. Weak updraft near the surface could not make the pollutants disperse in the vertical direction (Sun et al., 2017; Yin and  
Wang, 2018). During non-haze events, there appeared descending motion at the back of the AANA, while ascending motion  
was in the front. Through the direct vertical circulation, pollutants and water vapor were transported to the ocean. Drier  
atmosphere restrained the growth of fine particles. In brief, the vertical circulation between land and sea triggered by the  
AANA provided a stable source of water vapor for severe haze and weakened the turbulence. These might explain why severe



215 haze tended to last for a long time.

We further investigated the evolution processes of the AANA on severe haze/non-haze episodes to provide a basis for air quality forecast. Before severe haze episodes, Northeast Asia was mainly occupied by cyclonic circulation, which had the tendency of weakening over time (Figure 10a–c). This effect was caused by the strengthening of positive anomalies in Lake Baikal. The forward motion of positive anomalies in Lake Baikal was a precursory signal of severe haze. On the first day of severe haze, the AANA was relatively typical and strong at the mid-level, with anomalous southeasterly wind near the surface, bringing moisture to the BTH region (Figure 10d). One day after severe haze, the AANA moved to the east, and the main supply of water vapor began to change from southeasterly wind to low-level convergence (Figure 10f). Meanwhile, convergence in the low level could motivate sinking motion and lead to lower PBLH, which might trigger persistent haze. Three days after severe haze, the AANA was broken by cyclonic circulation and haze pollution tended to dissipate (Figure 10g). The rebuilt of cyclonic circulation in the BTH region represented the end of severe haze. For the non-haze episodes, the AANA remained strong and moved slowly before the non-haze day (Figure 10h–j). Few cyclones developed, which were mainly located in the high-latitude area. The switch from anomalous anticyclonic circulation to cyclonic anomalies occurred a day before the non-haze day, which was associated with polar cold air entering into the BTH region. On the first non-haze day, cyclonic circulation developed in Northeast Asia, which strengthened the prevailing northwesterly wind (Figure 10k). The anomalous northerly wind was conducive to the dissipation of pollutants. One day after the non-haze day, the cyclonic circulation in Northeast Asia developed, which was then forced to move eastward by the positive anomaly in Lake Baikal (Figure 10l–n). In brief, the emergence and development of severe haze (non-haze) was matched by the movements of the AANA. Thus, the AANA could be an effective forecast indicator for air quality.

#### 4. Conclusions and discussions

235 Severe haze in the BTH region has become more serious and persistent in recent years, which has wreaked havoc on society and economy. This research concentrated on severe haze episodes over the BTH region, occurring in December 2014–2016, which were identified by  $PM_{2.5}$  concentration data. Non-haze episodes were also taken into account as a comparison. The associated atmospheric circulations and the structure of the AANA were analyzed. The results indicated that the AANA was closely related to weaker surface wind, stronger temperature inversion, lower PBLH and higher relative humidity in the BTH region, which were of importance in the formation of severe haze. From the horizontal direction, the AANA motivated southeasterly wind in the lower troposphere, gathering pollutants and moisture to the BTH region. Strong southeaster also generated temperature inversion through warm advection, which strengthened the stability of lower atmosphere. In the vertical direction, the AANA generated ascending motion over the BTH region. Thus, there appeared anomalous updraft in the synoptic processes, which broke the local meridional circulation and restricted the transportation of clean air from the upper troposphere.



245 This phenomenon was a key factor of severe haze. Meanwhile, ascending motion restrained the downward transport of momentum and resulted in weaker surface wind speed and shallower PBL, which were highly detrimental to pollutant dispersion and strengthened the development of severe haze. The AANA also triggered an indirect circulation between land and sea, which acted as the main moisture path. Abundant moisture promoted the growth of haze particles and weakened the turbulence, providing favorable conditions for the emergence and development of severe haze. The evolution processes of the

250 AANA on severe haze/non-haze episodes were also discussed. The positive anomalies in Lake Baikal stretched eastward continuously before the AANA occupied Northeast Asia, which was a precursory signal of severe haze. In contrast, the transition from anticyclonic circulation to cyclonic circulation occurred a day before the non-haze day for the rapid movement of polar cold air.

The severe and non-haze events analyzed in this research were sorted out according to  $PM_{2.5}$  concentration. Compared

255 with visibility used in previous research (Chen and Wang, 2015; Yin et al., 2015a; Yin et al., 2015b), the  $PM_{2.5}$  concentration could represent the characteristics of haze episodes better. The basic results that weaker EAWM could lead to severe haze by generating weaker surface wind, stronger temperature inversion and higher relative humidity were in agreement with previous studies (Yin et al., 2015a; Yin and Wang, 2017b). In addition, this study offered novel insights into the formation of severe haze in the BTH region. Our analysis demonstrated the dynamic mechanism of how the AANA affected severe haze in the

260 BTH region. The AANA not only motivated southerly wind in the horizontal direction but also generated anomalous vertical motion composed of ascending branches at the back and descending branches in the front. These effects led to conducive local meteorological conditions for severe haze, including weaker surface wind, stronger temperature inversion, shallower PBL and higher relative humidity. In the different years, the relationship between the AANA and severe haze in the BTH region expressed different features but remained strong. In 2014 and 2016, the SPCCs between the  $PM_{2.5}$  concentration and

265  $AANAI_{Z500}$  ( $AANAI_{V850}$ ) were 0.76 (-0.66) and 0.76 (-0.66), respectively, both passing the 99% confidence level (Table 4). These results indicated that the AANA was relatively strong in the mid and lower troposphere and played an indicative role in the formation of severe haze over the BTH region in 2014 and 2016. However, the SPCC between the  $PM_{2.5}$  concentration and the  $AANAI_{Z500}$  was 0.22 in 2015, and it failed to pass the confidence test. Although the AANA was not evident in the geopotential field, it still emerged and had an impact on severe haze. The SPCC between the  $PM_{2.5}$  concentration and

270  $AANAI_{V850}$  ( $AANAI_{\theta500}$ ) was -0.54 (-0.50), exceeding the 95% confidence level (Table 4). In addition, there were some differences on how the AANA affected severe haze. In 2014, the AANA strengthened the severe haze mainly by enhancing surface relative humidity and TIP, whose SPCCs with the  $AANAI_{Z500}$  were 0.59 and 0.42, respectively (Table 4). Nevertheless, the AANA primarily promoted weaker surface wind in 2015. The SPCC between the  $AANAI_{Z500}$  and surface wind speed was -0.63 (Table 4). The impact of the AANA was typical in 2016, leading to lower surface wind speed and PBLH and higher

275 surface relative humidity and TIP. The SPCCs between the  $AANAI_{Z500}$  and surface wind speed, surface relative humidity, TIP,



and PBLH anomalies were -0.53, 0.68, 0.50, and -0.42, respectively (Table 4). These results might explain why haze pollution was more severe in 2016. The ascending motion at the back of the AANA might be corresponded with anomalous Hadley circulation, but it requires further research to confirm. Higher relative humidity could be verified in the upper level (200-300 hPa) because evaporated water vapor over the ocean could be brought to land by anomalous easterly wind. Further research remains necessary to explore how higher relative humidity in the upper troposphere affects severe haze. The evolution processes of the AANA on severe haze/non-haze episodes illustrated that the intensity of the AANA could play an indicative role in the emergence and dissipation of severe haze. However, the severe haze/non-haze events analyzed in this study were limited to the period of December 2014-2016. Further analysis containing more sample data is required to confirm whether the three AANAs we defined in this study could be reliable forecast indicators.

285

#### Acknowledgements:

This research was supported by the National Key Research and Development Plan (2016YFA0600703), the National Natural Science Foundation of China (41705058 and 91744311), the funding of Jiangsu innovation & entrepreneurship team, the CAS-PKU Partnership Program, 2017 Jiangsu Province College Students Innovation and Entrepreneurship Training Program (201710300007), and the Priority Academic Program Development (PAPD) of Jiangsu Higher Education Institutions.

290

#### References

- Betts, A. K.: The Parameterization of Deep Convection. The Physics and Parameterization of Moist Atmospheric Convection. Springer, Netherlands, 255-279, 1997.
- Chen, H. P. and Wang, H. J.: Haze Days in North China and the associated atmospheric circulations based on daily visibility data from 1960 to 2012. *J. Geophys. Res.*, **120**, 5895-5909, doi:10.1002/2015JD023225, 2015.
- Cai, W. J., Li, K., Liao, H., et al.: Weather conditions conducive to Beijing severe haze more frequent under climate change. *Nature Climate Change*, **7**, 257-262, doi:10.1038/nclimate3249, 2017.
- Ding, Y. H. and Liu, Y. J.: Analysis of long-term variations of fog and haze in China in recent 50 years and their relations with atmospheric humidity. *SCIENCE CHINA Earth Sciences*, **57**, 36-46, doi:10.1007/s11430-013-4792-1, 2014.
- “Formation Mechanism and Control Strategies of Haze in China” professional group.: Assessment report on PM<sub>2.5</sub> control effects in the Beijing-Tianjin-Hebei region since the implement of Air Pollution Prevention and Control Action Plan. *Bulletin of Chinese Academy of Sciences*, **30**, 668-678, doi:10.16418/j.issn.1000-3045.2015.05.012, 2015.
- He, S. P. and Wang, H. J.: An Integrated East Asian Winter Monsoon Index and Its Interannual Variability. *Chinese Journal of Atmospheric Sciences*, **36**, 523-538, doi:10.3878/j.issn.1006-9895.2011.11083, 2012.
- Hu, B., Chen, R., Xu, J. X., et al.: Health effects of ambient ultrafine (nano) particles in haze. *Chinese Science Bulletin*, **60**, 2808-2823, doi:10.1360/N972014-01404, 2015.
- Li, Q., Zhang, R. H., Wang, Y.: Interannual variation of the winter-time fog-haze days across central and eastern China and its relation with East Asian winter monsoon. *International Journal of Climatology*, **36**, 346-354, doi:10.1002/joc.4350, 2015.

305



- Liu, S. K. and Liu, S. D.: Atmospheric dynamics. 2nd ed., Peking University Press, Beijing, China, 143-147, 2011.
- 310 Liu, T. T., Gong, S. L., He, J. J., et al.: Attributions of meteorological and emission factors to the 2015 winter severe haze pollution episodes in China's Jing-Jin-Ji area. *Atmos. Chem. Phys.*, **17**, 2971-2980, doi:10.5194/acp-17-2971-2017, 2017.
- Lu, C. S., N, S. J., Yang, J., et al.: Jump Features and Causes of Macro and Microphysical Structures of a Winter Fog in Nanjing. *Chinese Journal of Atmospheric Sciences*, **34**, 681-690, doi:10.3878/j.issn.1006-9895.2010.04.02, 2010.
- 315 Sun, X. C., Han, Y. Q., Li, J., et al.: Analysis of the Influence of Vertical Movement on the Process of Fog and Haze with Air Pollution. *Plateau Meteorology*, **36**, 1106-1114, doi:10.7522/j.issn.1000-0534.2016.00076, 2017.
- Tang, B. Y., Xin, J. Y., Gao, W. K., et al.: Characteristics of complex air pollution in typical cities of North China. *Atmospheric and Oceanic Science Letters*, **11**, 29-36, doi:10.1080/16742834.2018.1394158, 2018.
- Wang, Y. S., Yao, L., Liu, Z. R., et al.: Formation of haze pollution in Beijing-Tianjin-Hebei region and their control strategies. *Bulletin of Chinese Academy of Sciences*, **28**, 353-363, doi:10.3969/j.issn.1000-3045.2013.03.009, 2013.
- 320 Wang, H. J., Chen, H. P. and Liu, J. P.: Arctic sea ice decline intensified haze pollution in eastern China. *Atmospheric and Oceanic Science Letters*, **8**, 1-9, doi:10.3878/AOSL20140081, 2015.
- Wang, H. J., Jiang, D. B.: A new East Asian winter monsoon intensity index and atmospheric circulation comparison between strong and weak composite. *Quaternary Sciences*, **24**, 19-27, doi:10.3321/j.issn:1001-7410.2004.01.003, 2004.
- 325 Wang, G. H., Zhang, R. Y., Gomez, M. E., et al.: Persistent sulfate formation from London Fog to Chinese haze. *Proceedings of the National Academy of Science*, **113**, 13630-13635, doi:10.1073/pnas.1616540113, 2016.
- Wang, H. J.: On assessing haze attribution and control measures in China. *Atmospheric and Oceanic Science Letters*, **11**, 120-122, doi:10.1080/16742834.2018.1409067, 2018.
- 330 Wei, Y., Li, J., Wang, Z. F., et al.: Trends of surface PM<sub>2.5</sub> over Beijing-Tianjin-Hebei in 2013-2015 and their causes: emission controls vs. meteorological conditions. *Atmospheric and Oceanic Science Letters*, **10**, 276-283, doi:10.1080/16742834.2017.1315631, 2017.
- Wu, P., Ding, Y. H., Liu, Y. J., et al.: Influence of the East Asian winter monsoon and atmospheric humidity on the wintertime haze frequency over central-eastern China. *Acta Meteorologica Sinica*, **74**, 352-366, doi:10.11676/qxb2016.029, 2016.
- Wu, P., Ding, Y. H. and Liu, Y. J.: Atmospheric circulation and dynamic mechanism for persistent haze events in the Beijing-Tianjin-Hebei region. *Advances in Atmospheric Sciences*, **34**, 429-440, doi:10.1007/s00376-016-6158-z, 2017.
- 335 Yang, T., Sun, Y. L., Zhang, W., et al.: Chemical characterization of submicron particles during typical air pollution episodes in spring over Beijing. *Atmospheric and Oceanic Science Letters*, **9**, 255-262, doi:10.1080/16742834.2016.1173509, 2016.
- Yin, Z. C., Wang, H. J. and Yuan, D. M.: Interdecadal increase of haze in winter over North China and the Huang-huai Area and the weakening of the East Asia Winter Monsoon. *Chinese Science Bulletin*, **60**, 1395-1400, doi:10.1360/N972014-01348, 2015a.
- 340 Yin, Z. C., Wang, H. J. and Guo, W. L.: Climatic change features of fog and haze in winter over North China and Huang-Huai Area. *SCIENCE CHINA Earth Sciences*, **58**, 1370-1376. doi:10.1007/s11430-015-5089-3, 2015b.
- Yin, Z. C. and Wang, H. J.: The relationship between the subtropical Western Pacific SST and haze over North-Central North China Plain. *International Journal of Climatology*, **36**, 3479-3491, doi:10.1002/joc.4570, 2016.
- 345 Yin, Z. C., Wang, H. J. and Chen, H. P.: Understanding severe winter haze events in the North China Plain in 2014: roles of climate anomalies. *Atmos. Chem. Phys.*, **17**, 1641-1651, doi:10.5194/acp-17-1641-2017, 2017a.
- Yin Z. C. and Wang H. J.: Role of Atmospheric Circulations on Haze Pollution in December 2016. *Atmos. Chem. Phys.*, **17**,



11673-11681, doi:10.5194/acp-17-11673-2017, 2017b.

Yin Z. C. and Wang H. J.: The Strengthening Relationship between Eurasian Snow Cover and December Haze Days in Central North China after the Mid-1990s. *Atmos. Chem. Phys.*, **18**, 4753-4763, doi:10.5194/acp-18-4753-2018, 2018

350 Zhao, X. J., Zhao, P. S., Xu, J., et al.: Analysis of a winter regional haze event and its formation mechanism in the North China Plain. *Atmos. Chem. Phys.*, **13**, 5685-5696, doi:10.5194/acp-13-5685-2013, 2013.

Zhang, X. Y., Sun, J. Y., Wang, Y. Q., et al.: Factors contributing to haze and fog in China. *Chinese Science Bulletin*, **58**, 1178-1187, doi:10.1360/972013-150, 2013.

355 Zhang, R. H., Li, Q. and Zhang, R. N.: Meteorological conditions for the persistent severe fog and haze event over eastern China in January 2013. *SCIENCE CHINA Earth Sciences*, **57**, 26-35, doi:10.1007/s11430-013-4774-3, 2014.

Zhang, Y. J., Zhang, P. Q., Wang, J., et al.: Climatic Characteristics of Persistent Haze Events over Jingjinji During 1981-2013. *Meteorological Monthly*, **41**, 311-318, doi:10.7519/j.issn.1000-0526.2015.03.006, 2015.

Zhong, Z., Yuan, H. H., Li, J., et al.: Characteristics of meso-scale perturbation and momentum transportation associated with an intensification process of upper-level jet. *Journal of the Meteorological Sciences*, **30**, 639-645, 2010.

360

#### Figure and table Captions:

365 **Table 1.** The timetable of 18 severe haze and 20 non-haze episodes. Note that the severe haze episodes are marked by gray shading. The units of concentration are  $\mu\text{g} \cdot \text{m}^{-3}$ . The start time and end time are all in Beijing local time.

370 **Table 2.** The SPCCs between the mean  $\text{PM}_{2.5}$  concentration over the BTH region and key indexes. All the SPCCs exceeded the 99% confidence level. The visibility, surface wind speed and surface relative humidity (RH) were based on observation data and calculated as the mean over the BTH region. The temperature inversion potential (TIP) was defined as  $T_{925} - T_{1000}$  and calculated as the mean over the BTH region. The planetary boundary layer height (PBLH) anomalies were calculated as the mean over  $35^{\circ}\text{-}40^{\circ}\text{N}$ ,  $110^{\circ}\text{-}120^{\circ}\text{E}$  and with respect to the period from 1979-2010.

**Table 3.** The SPCCs between  $\text{AANAI}_{Z500}$  ( $\text{AANAI}_{f850}$ ,  $\text{AANAI}_{\omega500}$ ) and regional meteorological indexes. “\*” represents that the SPCC exceeded the 95% confidence level, and “\*\*\*” represents that the SPCC exceeded the 99% confidence level.

375 **Table 4.** The SPCCs between the mean  $\text{PM}_{2.5}$  concentration over the BTH region and key indexes in December 2014, 2015 and 2016. “\*” represents that the SPCC exceeded the 95% confidence level, and “\*\*\*” represents that the SPCC exceeded the 99% confidence level.

**Table 5.** The SPCCs between  $\text{AANAI}_{Z500}$  ( $\text{AANAI}_{f850}$ ,  $\text{AANAI}_{\omega500}$ ) and regional meteorological indexes in December 2014, 2015 and 2016. “\*” represents that the SPCC exceeded the 95% confidence level, and “\*\*\*” represents that the SPCC exceeded the 99% confidence level.

380 **Figure 1.** The six-hour variation of mean  $\text{PM}_{2.5}$  concentration over the BTH region (units:  $\mu\text{g} \cdot \text{m}^{-3}$ ) in December 2014-2016. The time series (concentrations) corresponding to the red/blue line represent the occurrence time (threshold values) of severe haze/non-haze episodes.

**Figure 2.** Composite distribution of the atmospheric circulation anomalies on severe haze/non-haze episodes. The anomalies here are calculated with respect to the 1979-2010 climatology. The green (white) box indicates the BTH region (area covered by  $\text{AANAI}_{Z500}$ ). (a)  $Z_{500}$  (shading, units:  $\text{m}^2 \cdot \text{s}^{-2}$ ) and  $U_{200}$  (contour, units:  $\text{m} \cdot \text{s}^{-1}$ ) on severe haze episodes; the white dots



385 indicate that the  $Z_{500}$  anomalies exceeded the 95% confidence level. (b) SLP (shading, units: hPa) and SAT (contour, units: K) on severe haze episodes; the white dots indicate that the SLP anomalies exceeded the 95% confidence level. (c)  $Z_{500}$  (shading, units:  $m^2 \cdot s^{-2}$ ) and  $U_{200}$  (contour, units:  $m \cdot s^{-1}$ ) on non-haze episodes; the white dots indicate that the  $Z_{500}$  anomalies exceeded the 95% confidence level. (d) SLP (shading, units: hPa) and SAT (contour, units: K) on non-haze episodes; the white dots indicate that the SLP anomalies exceeded the 95% confidence level.

390 **Figure 3.** Composite distribution of local atmospheric circulation anomalies on severe haze/non-haze episodes. The anomalies here are calculated with respect to the 1979-2010 climatology. The green (black) box indicates the BTH region (area covered by AANA $_{V_{850}}$ ). (a)  $V_{850}$  (arrow, units:  $m \cdot s^{-1}$ ) and temperature inversion potential ( $T_{925}-T_{1000}$ , shading, units: K) on severe haze episodes; the white dots indicate that the temperature inversion potential anomalies exceeded the 95% confidence level. (b) Surface wind (arrow, units:  $m \cdot s^{-1}$ ) and surface relative humidity (shading, units: %) on severe haze episodes; the white dots indicate that the surface relative humidity anomalies exceeded the 95% confidence level. (c)  $V_{850}$  (arrow, units:  $m \cdot s^{-1}$ ) and temperature inversion potential ( $T_{925}-T_{1000}$ , shading, units: K) on non-haze episodes; the white dots indicate that the temperature inversion potential anomalies exceeded the 95% confidence level. (d) Surface wind (arrow, units:  $m \cdot s^{-1}$ ) and surface relative humidity (shading, units: %) on non-haze episodes; the white dots indicate that the surface relative humidity anomalies exceeded the 95% confidence level.

400 **Figure 4.** The six-hour variation of  $PM_{2.5}$  concentration and surface wind speed, surface relative humidity, and TIP in December 2014-2016. The data were processed by min-max normalization. The time series corresponding to red/blue shading represent the occurrence time of severe haze/non-haze episodes.

**Figure 5.** The six-hour variation of  $PM_{2.5}$  concentration, AANA $_{Z_{500}}$ , AANA $_{V_{850}}$ , and AANA $_{\omega_{500}}$  in December 2014-2016. The time series corresponding to red/blue shading represent the occurrence time of severe haze/non-haze episodes.

405 **Figure 6.** Structure of AANA in the mid-level:  $Z_{500}$  (contour, units:  $m^2 \cdot s^{-2}$ ) and  $\omega_{500}$  (shading, units:  $Pa \cdot s^{-1}$ ). The anomalies here are calculated with respect to the 1979-2010 climatology. The green (white) box indicates the BTH region (area covered by AANA $_{\omega_{500}}$ ). (a) severe haze episodes, (b) non-haze episodes. The white dots indicate that the  $\omega_{500}$  anomalies exceeded the 95% confidence level.

**Figure 7.** Vertical distribution of temperature advection (units:  $10^{-5}K \cdot s^{-1}$ ) over the BTH region. The black line represents the differences between severe haze and non-haze. “⊗” indicates that the differences of temperature advection between severe haze and non-haze exceeded the 95% confidence level.

**Figure 8.** Vertical section on severe haze/non-haze episodes (composite anomalies): (a) Vertical cross section (115°-125°E mean) of wind anomalies (omega, shading, units:  $Pa \cdot s^{-1}$ ; wind, arrow, omega magnified 100 times, units:  $m \cdot s^{-1}$ ) and PBLH anomalies (contour, units: m) on severe haze episodes; the left coordinate is pressure level and the right coordinate is PBLH anomaly; the white dots indicate that the omega anomalies exceeded the 95% confidence level. (b) Zonal vertical section (36°-42°N mean) of wind anomalies (omega, shading, units:  $Pa \cdot s^{-1}$ ; wind, arrow, omega magnified 100 times, units:  $m \cdot s^{-1}$ ) and relative humidity anomalies (contour, units: %) on severe haze episodes; the white dots indicate that the omega anomalies exceeded the 95% confidence level. (c) Vertical cross section (115°-125°E mean) of wind anomalies (omega, shading, units:  $Pa \cdot s^{-1}$ ; wind, arrow, omega magnified 100 times, units:  $m \cdot s^{-1}$ ) and PBLH anomalies (contour, units: m) on non-haze episodes; the left coordinate is the pressure level, and the right coordinate is the PBLH anomaly; the white dots indicate that the omega anomalies exceeded the 95% confidence level. (d) Zonal vertical section (36°-42°N mean) of wind anomalies (omega, shading, units:  $Pa \cdot s^{-1}$ ; wind, arrow, omega magnified 100 times, units:  $m \cdot s^{-1}$ ) and relative humidity (contour, units: %) on non-haze episodes; the white dots indicate that the omega anomalies exceeded the 95% confidence level. The anomalies here are calculated with respect to the 1979-2010 climatology. To make the horizontal velocity and the vertical velocity in the same order, the vertical velocity (omega) here is magnified 100 times.

**Figure 9.** Vertical section on severe haze/non-haze episodes (composite synoptic processes): (a) Vertical cross section (114°-120°E mean) of wind (omega, shading, units:  $Pa \cdot s^{-1}$ ; wind, arrow, omega magnified 100 times, units:  $m \cdot s^{-1}$ ) on severe



haze episodes; the white dots indicate that omega exceeded the 95% confidence level. (b) Zonal vertical section (36°-42°N  
430 mean) of wind (arrow, omega magnified 100 times, units:  $\text{m} \cdot \text{s}^{-1}$ ) and the vertical transport of westerly momentum (shading,  
units:  $10^{-3} \text{m} \cdot \text{s}^{-2}$ ) on severe haze episodes; the white dots indicate that the vertical transport of westerly momentum  
exceeded the 95% confidence level. (c) Vertical cross section (114°-120°E mean) of wind (omega, shading, units:  $\text{Pa} \cdot \text{s}^{-1}$ ;  
wind, arrow, omega magnified 100 times, units:  $\text{m} \cdot \text{s}^{-1}$ ) on non-haze episodes; the white dots indicate that omega exceeded  
the 95% confidence level. (d) Zonal vertical section (36°-42°N mean) of wind (arrow, omega magnified 100 times,  
435 units:  $\text{m} \cdot \text{s}^{-1}$ ) and the vertical transport of westerly momentum (shading, units:  $10^{-3} \text{m} \cdot \text{s}^{-2}$ ) on non-haze episodes; the  
white dots indicate that the vertical transport of westerly momentum exceeded the 95% confidence level. To make the  
horizontal velocity and the vertical velocity in the same order, the vertical velocity (omega) here is magnified 100 times.

**Figure 10.** Evolution of the AANA on severe haze episodes (a-g) and non-haze episodes (h-n):  $Z_{500}$  (shading, units:  $\text{m}^2 \cdot \text{s}^{-2}$ )  
and wind at 850 hPa (arrow, units:  $\text{m} \cdot \text{s}^{-1}$ ). The anomalies here are calculated with respect to the 1979-2010 climatology.  
Severe haze/non-haze day+0 refers to the first day of severe haze/non-haze. Severe haze (non-haze) day-3, severe haze (non-  
440 haze) day-2, and severe haze (non-haze) day-1 refer to three, two, and one day(s) before the first day of severe haze (non-haze),  
respectively. Severe haze (non-haze) day+1, severe haze (non-haze) day+2, and severe haze (non-haze) day+3 refer to one,  
two, and three day(s) after the first day of severe haze (non-haze), respectively. The green, white and black boxes indicate the  
BTH region and areas covered by  $\text{AANA}_{Z_{500}}$  and  $\text{AANA}_{P_{850}}$ , respectively.



445 **Table 1.** The timetable of 18 severe haze and 20 non-haze episodes. Note that the severe haze episodes are marked by gray shading. The units of concentration are  $\mu\text{g} \cdot \text{m}^{-3}$ . The start time and end time are all in Beijing local time.

Year	Start time	End time	Mean concentration	Start time	End time	Mean concentration
2014	1 <sup>st</sup> 08 <sup>00</sup>	2 <sup>nd</sup> 08 <sup>00</sup>	32.7	15 <sup>th</sup> 20 <sup>00</sup>	17 <sup>th</sup> 02 <sup>00</sup>	24.3
	2 <sup>nd</sup> 20 <sup>00</sup>	5 <sup>th</sup> 14 <sup>00</sup>	36.9	18 <sup>th</sup> 20 <sup>00</sup>	19 <sup>th</sup> 08 <sup>00</sup>	156.2
	9 <sup>th</sup> 20 <sup>00</sup>	10 <sup>th</sup> 08 <sup>00</sup>	189.8	19 <sup>th</sup> 20 <sup>00</sup>	21 <sup>st</sup> 20 <sup>00</sup>	31.6
	10 <sup>th</sup> 20 <sup>00</sup>	11 <sup>th</sup> 14 <sup>00</sup>	37.8	23 <sup>rd</sup> 20 <sup>00</sup>	24 <sup>th</sup> 02 <sup>00</sup>	170.2
	12 <sup>th</sup> 08 <sup>00</sup>	12 <sup>th</sup> 20 <sup>00</sup>	26.3	24 <sup>th</sup> 20 <sup>00</sup>	24 <sup>th</sup> 20 <sup>00</sup>	48.9
	13 <sup>th</sup> 14 <sup>00</sup>	13 <sup>th</sup> 14 <sup>00</sup>	47.0	27 <sup>th</sup> 02 <sup>00</sup>	28 <sup>th</sup> 14 <sup>00</sup>	210.8
	15 <sup>th</sup> 02 <sup>00</sup>	15 <sup>th</sup> 08 <sup>00</sup>	173.3	31 <sup>st</sup> 02 <sup>00</sup>	31 <sup>st</sup> 20 <sup>00</sup>	28.2
	1 <sup>st</sup> 08 <sup>00</sup>	2 <sup>nd</sup> 02 <sup>00</sup>	200.1	20 <sup>th</sup> 20 <sup>00</sup>	25 <sup>th</sup> 02 <sup>00</sup>	234.2
2015	2 <sup>nd</sup> 14 <sup>00</sup>	4 <sup>th</sup> 20 <sup>00</sup>	26.4	25 <sup>th</sup> 14 <sup>00</sup>	26 <sup>th</sup> 08 <sup>00</sup>	185.7
	7 <sup>th</sup> 20 <sup>00</sup>	10 <sup>th</sup> 08 <sup>00</sup>	219.6	27 <sup>th</sup> 02 <sup>00</sup>	27 <sup>th</sup> 14 <sup>00</sup>	25.1
	11 <sup>th</sup> 14 <sup>00</sup>	11 <sup>th</sup> 14 <sup>00</sup>	48.5	29 <sup>th</sup> 02 <sup>00</sup>	29 <sup>th</sup> 02 <sup>00</sup>	150.4
	15 <sup>th</sup> 08 <sup>00</sup>	17 <sup>th</sup> 14 <sup>00</sup>	23.7	29 <sup>th</sup> 14 <sup>00</sup>	30 <sup>th</sup> 08 <sup>00</sup>	217.4
	1 <sup>st</sup> 14 <sup>00</sup>	1 <sup>st</sup> 14 <sup>00</sup>	30.9	14 <sup>th</sup> 08 <sup>00</sup>	14 <sup>th</sup> 14 <sup>00</sup>	37.3
2016	2 <sup>nd</sup> 20 <sup>00</sup>	3 <sup>rd</sup> 02 <sup>00</sup>	153.2	17 <sup>th</sup> 02 <sup>00</sup>	17 <sup>th</sup> 02 <sup>00</sup>	150.8
	3 <sup>rd</sup> 14 <sup>00</sup>	5 <sup>th</sup> 02 <sup>00</sup>	210.6	17 <sup>th</sup> 14 <sup>00</sup>	22 <sup>nd</sup> 02 <sup>00</sup>	240.0
	5 <sup>th</sup> 14 <sup>00</sup>	5 <sup>th</sup> 20 <sup>00</sup>	44.2	23 <sup>rd</sup> 08 <sup>00</sup>	23 <sup>rd</sup> 14 <sup>00</sup>	39.8
	9 <sup>th</sup> 02 <sup>00</sup>	9 <sup>th</sup> 20 <sup>00</sup>	33.2	25 <sup>th</sup> 20 <sup>00</sup>	26 <sup>th</sup> 02 <sup>00</sup>	162.1
	11 <sup>th</sup> 20 <sup>00</sup>	12 <sup>th</sup> 20 <sup>00</sup>	175.9	27 <sup>th</sup> 14 <sup>00</sup>	27 <sup>th</sup> 14 <sup>00</sup>	47.7
	13 <sup>th</sup> 14 <sup>00</sup>	13 <sup>th</sup> 20 <sup>00</sup>	39.2	30 <sup>th</sup> 14 <sup>00</sup>	31 <sup>st</sup> 20 <sup>00</sup>	209.8



**Table 2.** The SPCCs between the mean  $PM_{2.5}$  concentration over the BTH region and key indexes. All the SPCCs exceeded the 99% confidence level. The visibility, surface wind speed and surface relative humidity (RH) were based on observation data and calculated as the mean over the BTH region. The temperature inversion potential (TIP) was defined as  $T_{925}-T_{1000}$  and calculated as the mean over the BTH region. The planetary boundary layer height (PBLH) anomalies were calculated as the mean over  $35^{\circ}-40^{\circ}N$ ,  $110^{\circ}-120^{\circ}E$  and with respect to the period from 1979-2010.

Index	AANA $I_{Z500}$	AANA $I_{V850}$	AANA $I_{\omega 500}$	Visibility	Surface wind speed	Surface RH	TIP	PBLH anomalies
SPCC	0.57	-0.64	-0.60	-0.83	-0.41	0.73	0.63	-0.38

**Table 3.** The SPCCs between  $AANA_{I_{Z500}}$  ( $AANA_{I_{V850}}$ ,  $AANA_{I_{\omega 500}}$ ) and regional meteorological indexes. “\*” represents that the SPCC exceeded the 95% confidence level, and “\*\*” represents that the SPCC exceeded the 99% confidence level.

SPCC	Visibility	Surface wind speed	Surface RH	TIP	PBLH anomalies
$AANA_{I_{Z500}}$	-0.62**	-0.41**	0.65**	0.39**	-0.48**
$AANA_{I_{V850}}$	0.59**	0.20	-0.55**	-0.38**	0.17
$AANA_{I_{\omega 500}}$	0.46**	0.04	-0.44**	-0.40**	-0.03

**Table 4.** The SPCCs between the mean  $PM_{2.5}$  concentration over the BTH region and key indexes in December 2014, 2015 and 2016. “\*” represents that the SPCC exceeded the 95% confidence level, and “\*\*” represents that the SPCC exceeded the 99% confidence level.

SPCC	AANA $I_{500}$	AANA $I_{850}$	AANA $I_{\omega 500}$	Visibility	Surface wind speed	Surface RH	TIP	PBLH anomalies
2014	0.76**	-0.66**	-0.70**	-0.79**	-0.33	0.75**	0.63**	-0.39*
2015	0.22	-0.54*	-0.50*	-0.88**	-0.51*	0.83**	0.49*	-0.27
2016	0.76**	-0.66**	-0.61**	-0.88**	-0.55**	0.80**	0.70**	-0.44*

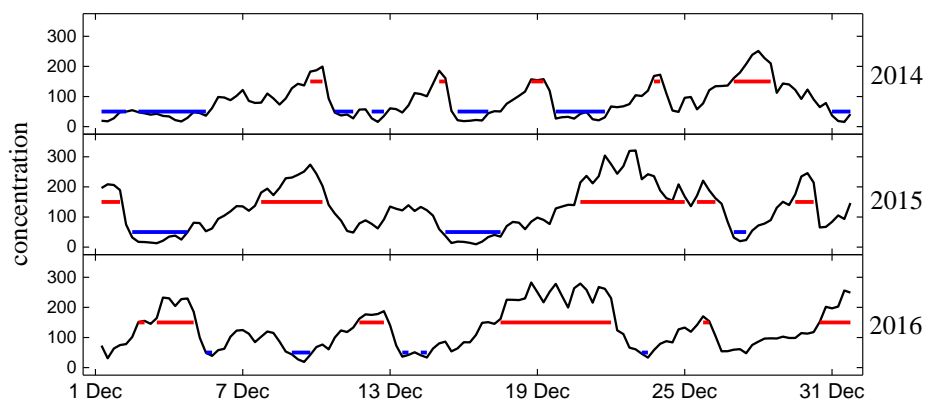
460



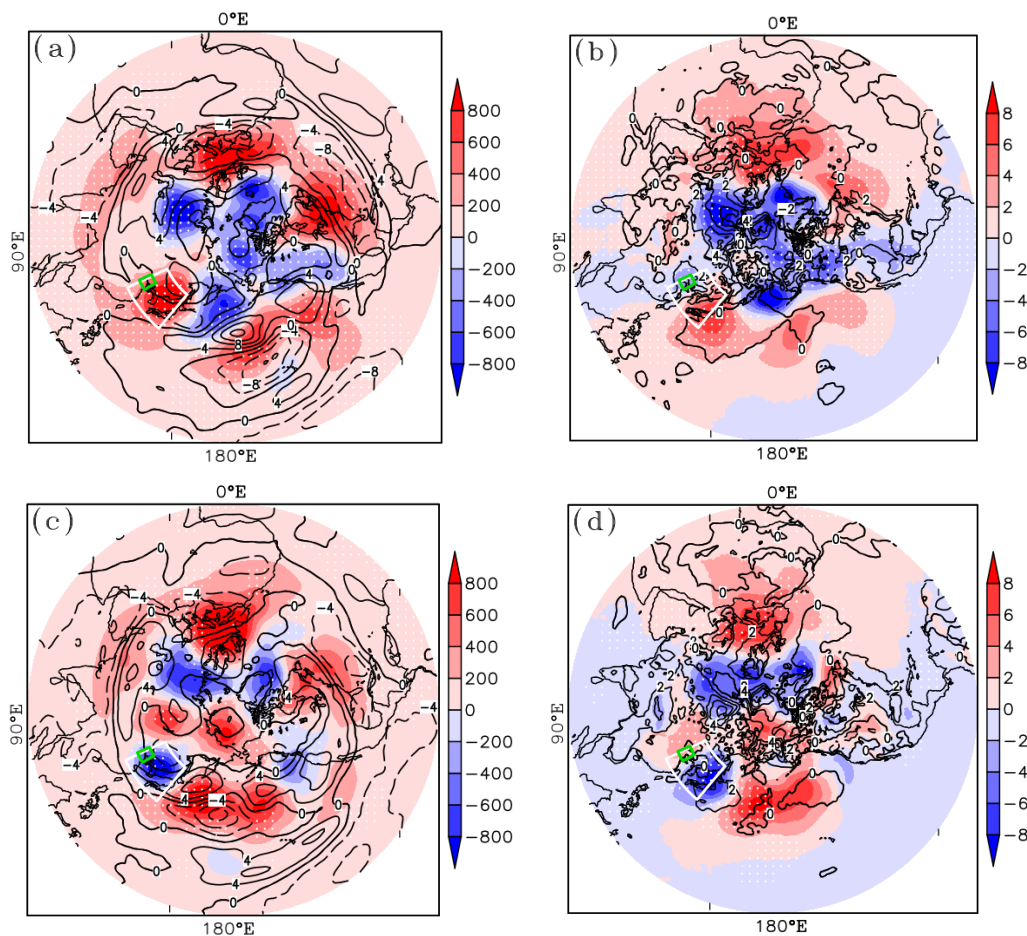
**Table 5.** The SPCCs between AANAI<sub>Z500</sub> (AANAI<sub>r850</sub>, AANAI<sub>ω500</sub>) and regional meteorological indexes in December 2014, 2015 and 2016. “\*” represents that the SPCC exceeded the 95% confidence level, and “\*\*” represents that the SPCC exceeded the 99% confidence level.

Year	SPCC	Visibility	Surface wind speed	Surface RH	TIP	PBLH anomalies
2014	AANAI <sub>Z500</sub>	-0.56**	-0.10	0.59**	0.42*	-0.18
	AANAI <sub>r850</sub>	0.34	-0.15	-0.36	-0.22	-0.01
	AANAI <sub>ω500</sub>	0.43*	-0.16	-0.43*	-0.31	-0.18
2015	AANAI <sub>Z500</sub>	-0.21	-0.63**	0.12	-0.28	-0.48*
	AANAI <sub>r850</sub>	0.62**	0.56*	-0.57**	-0.26	0.08
	AANAI <sub>ω500</sub>	0.54*	0.37	-0.53*	-0.25	0.05
2016	AANAI <sub>Z500</sub>	-0.71**	-0.53**	0.68**	0.50**	-0.42*
	AANAI <sub>r850</sub>	0.72**	0.47*	-0.66**	-0.43**	0.30
	AANAI <sub>ω500</sub>	0.57**	0.33	-0.63**	-0.57**	0.11

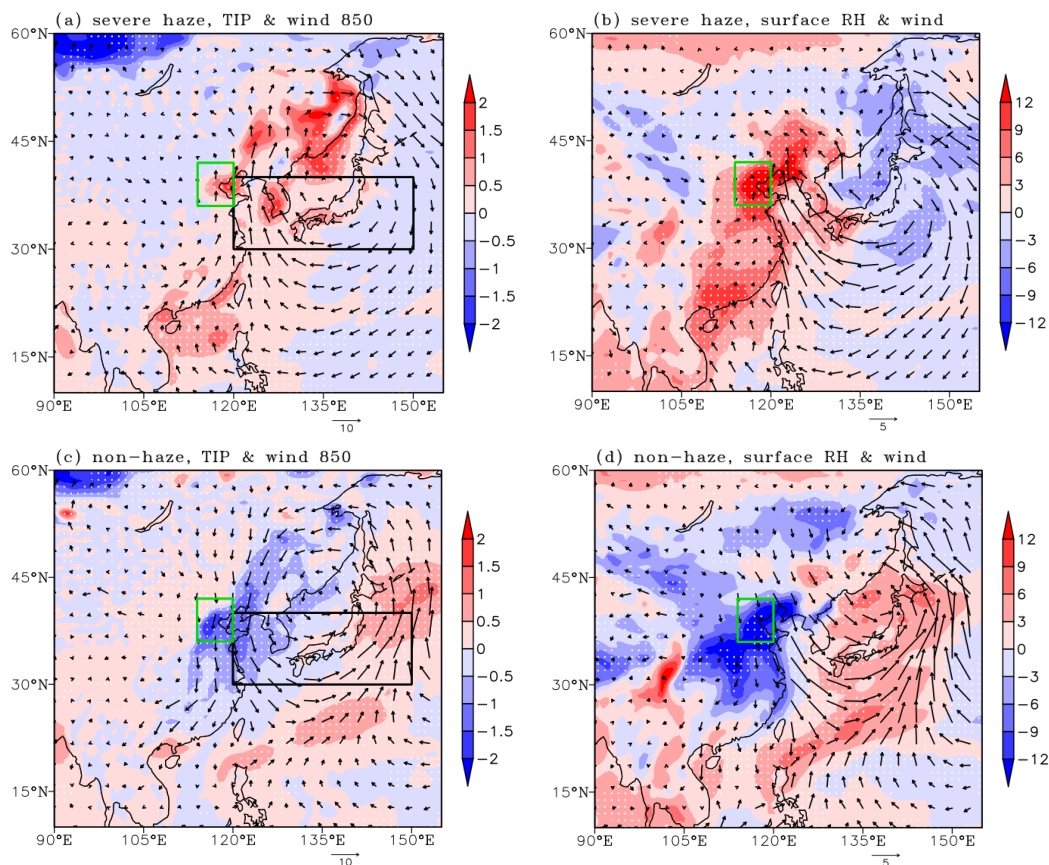
465



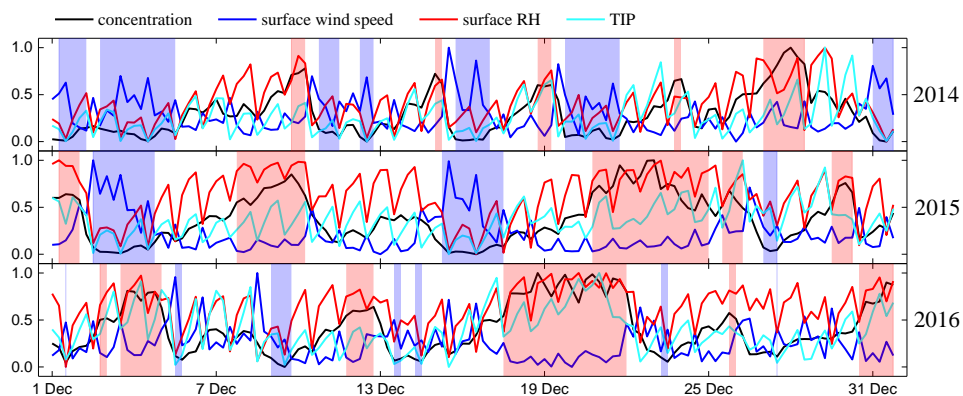
**Figure 1.** The six-hour variation of mean PM<sub>2.5</sub> concentration over the BTH region (units:  $\mu\text{g} \cdot \text{m}^{-3}$ ) in December 2014–2016. The time series (concentrations) corresponding to the red/blue line represent the occurrence time (threshold values) of severe haze/non-haze episodes.



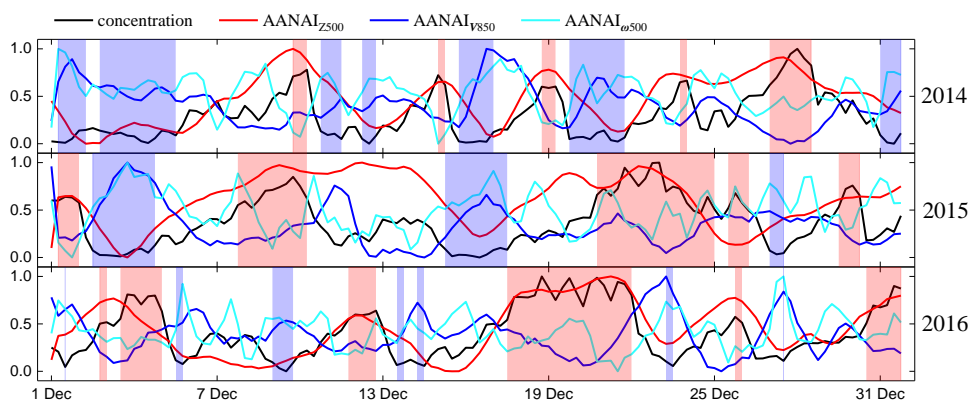
**Figure 2.** Composite distribution of the atmospheric circulation anomalies on severe haze/non-haze episodes. The anomalies here are calculated with respect to the 1979-2010 climatology. The green (white) box indicates the BTH region (area covered by AANA<sub>I<sub>Z500</sub></sub>). (a)  $Z_{500}$  (shading, units:  $m^2 \cdot s^{-2}$ ) and  $U_{200}$  (contour, units:  $m \cdot s^{-1}$ ) on severe haze episodes; the white dots indicate that the  $Z_{500}$  anomalies exceeded the 95% confidence level. (b) SLP (shading, units: hPa) and SAT (contour, units: K) on severe haze episodes; the white dots indicate that the SLP anomalies exceeded the 95% confidence level. (c)  $Z_{500}$  (shading, units:  $m^2 \cdot s^{-2}$ ) and  $U_{200}$  (contour, units:  $m \cdot s^{-1}$ ) on non-haze episodes; the white dots indicate that the  $Z_{500}$  anomalies exceeded the 95% confidence level. (d) SLP (shading, units: hPa) and SAT (contour, units: K) on non-haze episodes; the white dots indicate that the SLP anomalies exceeded the 95% confidence level.



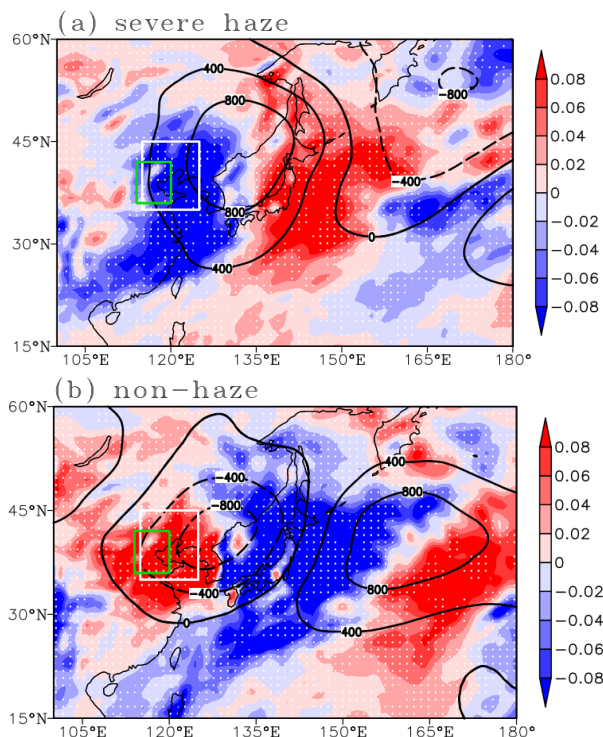
**Figure 3.** Composite distribution of local atmospheric circulation anomalies on severe haze/non-haze episodes. The anomalies here are calculated with respect to the 1979-2010 climatology. The green (black) box indicates the BTH region (area covered by AANAI<sub>850</sub>). (a)  $V_{850}$  (arrow, units:  $\text{m} \cdot \text{s}^{-1}$ ) and temperature inversion potential ( $T_{925}-T_{1000}$ , shading, units: K) on severe haze episodes; the white dots indicate that the temperature inversion potential anomalies exceeded the 95% confidence level. (b) Surface wind (arrow, units:  $\text{m} \cdot \text{s}^{-1}$ ) and surface relative humidity (shading, units: %) on severe haze episodes; the white dots indicate that the surface relative humidity anomalies exceeded the 95% confidence level. (c)  $V_{850}$  (arrow, units:  $\text{m} \cdot \text{s}^{-1}$ ) and temperature inversion potential ( $T_{925}-T_{1000}$ , shading, units: K) on non-haze episodes; the white dots indicate that the temperature inversion potential anomalies exceeded the 95% confidence level. (d) Surface wind (arrow, units:  $\text{m} \cdot \text{s}^{-1}$ ) and surface relative humidity (shading, units: %) on non-haze episodes; the white dots indicate that the surface relative humidity anomalies exceeded the 95% confidence level.



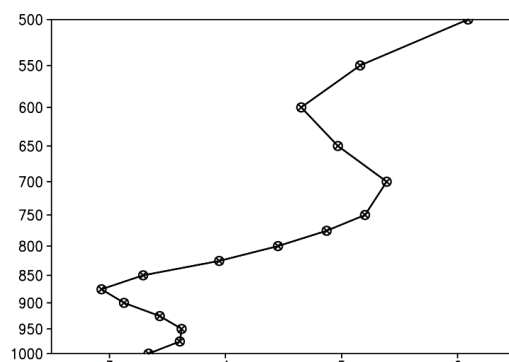
**Figure 4.** The six-hour variation of  $PM_{2.5}$  concentration and surface wind speed, surface relative humidity, and TIP in December 2014–2016. The data were processed by min-max normalization. The time series corresponding to red/blue shading represent the occurrence time of severe haze/non-haze episodes.



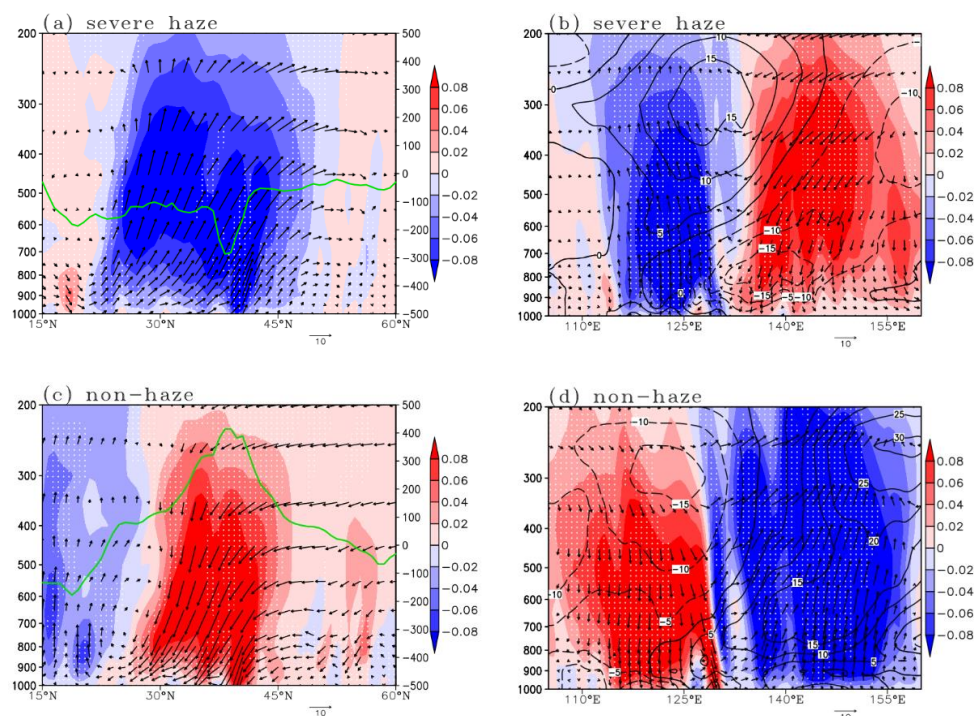
**Figure 5.** The six-hour variation of  $PM_{2.5}$  concentration,  $AANAI_{z500}$ ,  $AANAI_{v850}$ , and  $AANAI_{o500}$  in December 2014–2016. The time series corresponding to red/blue shading represent the occurrence time of severe haze/non-haze episodes.



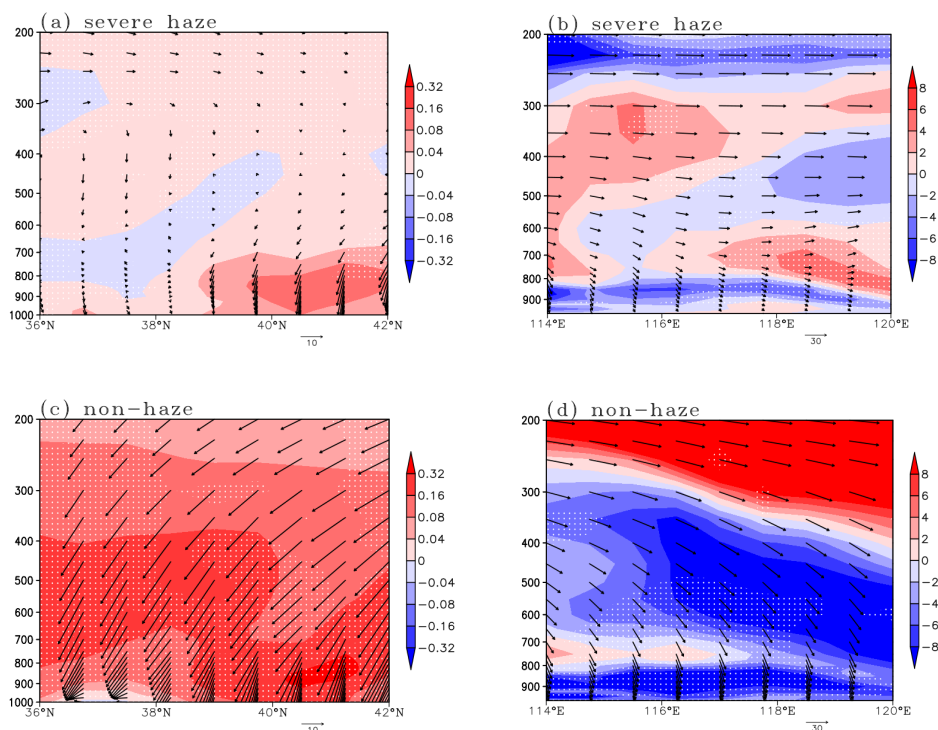
**Figure 6.** Structure of AANA in the mid-level:  $Z_{500}$  (contour, units:  $m^2 \cdot s^{-2}$ ) and  $\omega_{500}$  (shading, units:  $Pa \cdot s^{-1}$ ). The anomalies here are calculated with respect to the 1979–2010 climatology. The green (white) box indicates the BTH region (area covered by AANA $_{\omega_{500}}$ ). (a) severe haze episodes, (b) non-haze episodes. The white dots indicate that the  $\omega_{500}$  anomalies exceeded the 95% confidence level.



**Figure 7.** Vertical distribution of temperature advection (units:  $10^{-5} K \cdot s^{-1}$ ) over the BTH region. The black line represents the differences between severe haze and non-haze. “X” indicates that the differences of temperature advection between severe haze and non-haze exceeded the 95% confidence level.



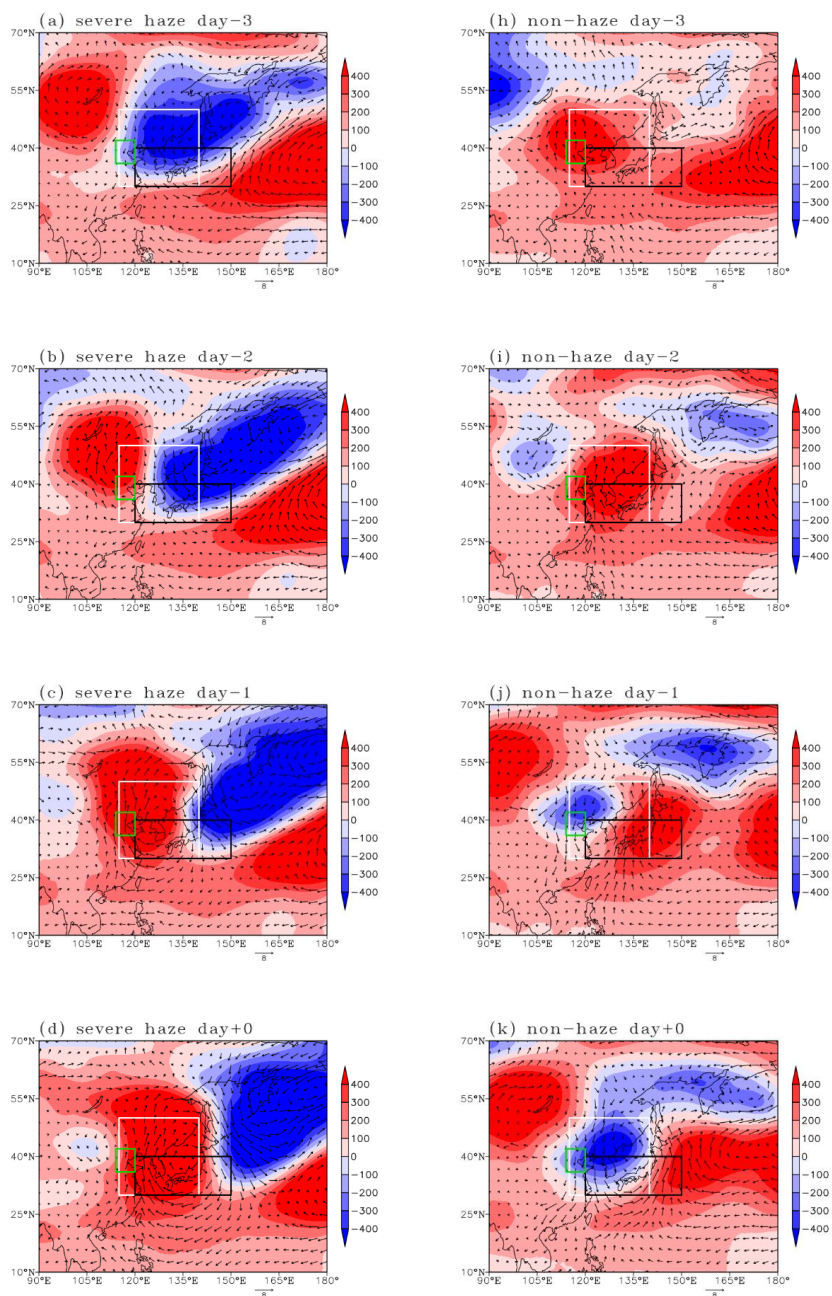
**Figure 8.** Vertical section on severe haze/non-haze episodes (composite anomalies): (a) Vertical cross section (115°-125°E mean) of wind anomalies (omega, shading, units: Pa · s<sup>-1</sup>; wind, arrow, omega magnified 100 times, units: m · s<sup>-1</sup>) and PBLH anomalies (contour, units: m) on severe haze episodes; the left coordinate is pressure level and the right coordinate is PBLH anomaly; the white dots indicate that the omega anomalies exceeded the 95% confidence level. (b) Zonal vertical section (36°-42°N mean) of wind anomalies (omega, shading, units: Pa · s<sup>-1</sup>; wind, arrow, omega magnified 100 times, units: m · s<sup>-1</sup>) and relative humidity anomalies (contour, units: %) on severe haze episodes; the white dots indicate that the omega anomalies exceeded the 95% confidence level. (c) Vertical cross section (115°-125°E mean) of wind anomalies (omega, shading, units: Pa · s<sup>-1</sup>; wind, arrow, omega magnified 100 times, units: m · s<sup>-1</sup>) and PBLH anomalies (contour, units: m) on non-haze episodes; the left coordinate is the pressure level, and the right coordinate is the PBLH anomaly; the white dots indicate that the omega anomalies exceeded the 95% confidence level. (d) Zonal vertical section (36°-42°N mean) of wind anomalies (omega, shading, units: Pa · s<sup>-1</sup>; wind, arrow, omega magnified 100 times, units: m · s<sup>-1</sup>) and relative humidity (contour, units: %) on non-haze episodes; the white dots indicate that the omega anomalies exceeded the 95% confidence level. The anomalies here are calculated with respect to the 1979-2010 climatology. To make the horizontal velocity and the vertical velocity in the same order, the vertical velocity (omega) here is magnified 100 times.



**Figure 9.** Vertical section on severe haze/non-haze episodes (composite synoptic processes): (a) Vertical cross section ( $114^{\circ}$ - $120^{\circ}$ E mean) of wind (omega, shading, units:  $\text{Pa} \cdot \text{s}^{-1}$ ; wind, arrow, omega magnified 100 times, units:  $\text{m} \cdot \text{s}^{-1}$ ) on severe haze episodes; the white dots indicate that omega exceeded the 95% confidence level. (b) Zonal vertical section ( $36^{\circ}$ - $42^{\circ}$ N mean) of wind (arrow, omega magnified 100 times, units:  $\text{m} \cdot \text{s}^{-1}$ ) and the vertical transport of westerly momentum (shading, units:  $10^{-3} \text{m} \cdot \text{s}^{-2}$ ) on severe haze episodes; the white dots indicate that the vertical transport of westerly momentum exceeded the 95% confidence level. (c) Vertical cross section ( $114^{\circ}$ - $120^{\circ}$ E mean) of wind (omega, shading, units:  $\text{Pa} \cdot \text{s}^{-1}$ ; wind, arrow, omega magnified 100 times, units:  $\text{m} \cdot \text{s}^{-1}$ ) on non-haze episodes; the white dots indicate that omega exceeded the 95% confidence level. (d) Zonal vertical section ( $36^{\circ}$ - $42^{\circ}$ N mean) of wind (arrow, omega magnified 100 times, units:  $\text{m} \cdot \text{s}^{-1}$ ) and the vertical transport of westerly momentum (shading, units:  $10^{-3} \text{m} \cdot \text{s}^{-2}$ ) on non-haze episodes; the white dots indicate that the vertical transport of westerly momentum exceeded the 95% confidence level. To make the horizontal velocity and the vertical velocity in the same order, the vertical velocity (omega) here is magnified 100 times.

480

485



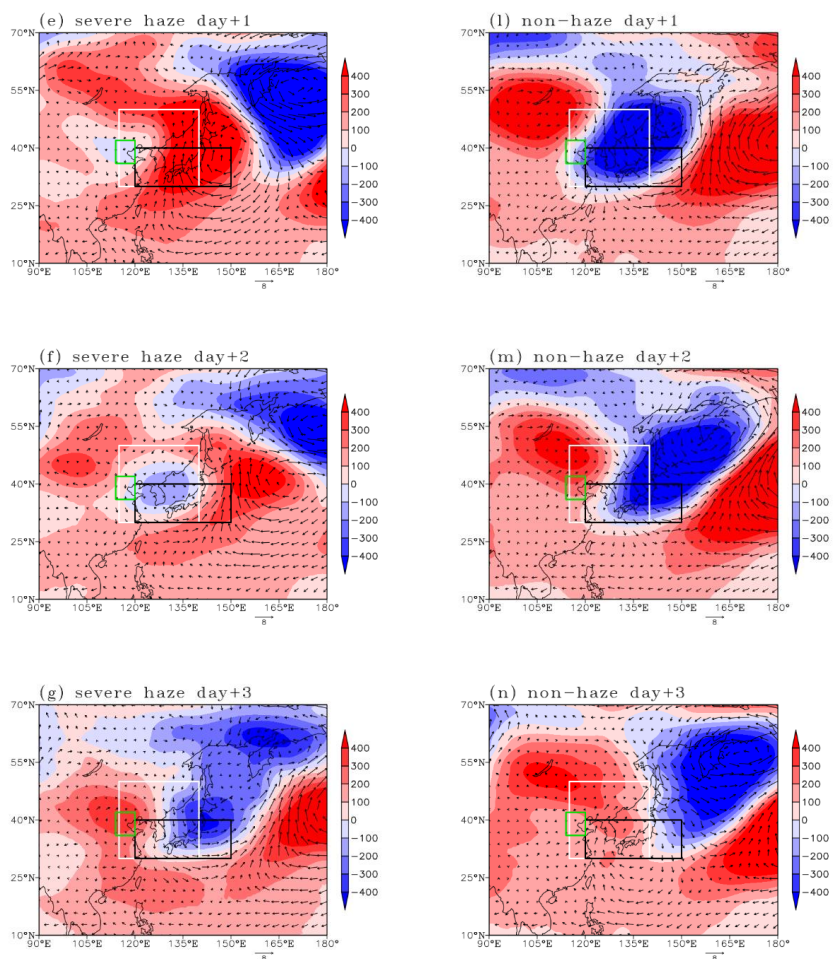


**Figure 10.** Evolution of the AANA on severe haze episodes (a-g) and non-haze episodes (h-n):  $Z_{500}$  (shading, units:  $m^2 \cdot s^{-2}$ ) and wind at 850 hPa (arrow, units:  $m \cdot s^{-1}$ ). The anomalies here are calculated with respect to the 1979-2010 climatology. Severe haze/non-haze day+0 refers to the first day of severe haze/non-haze. Severe haze (non-haze) day-3, severe haze (non-haze) day-2, and severe haze (non-haze) day-1 refer to three, two, and one day(s) before the first day of severe haze (non-haze), respectively. Severe haze (non-haze) day+1, severe haze (non-haze) day+2, and severe haze (non-haze) day+3 refer to one, two, and three day(s) after the first day of severe haze (non-haze), respectively. The green, white and black boxes indicate the BTH region and areas covered by  $AANA_{Z500}$  and  $AANA_{850}$ , respectively.